

# Reversible Thermochromic Bismuth Iodide Enabled by Self-Adjustment

Rui Wen, Yanyan Wang,\* Xinjie Ma, Yikun Yan, Qi Ma, Jinpeng Gao, Huaming Sun, Hao Huang,\* and Ziwei Gao\*

Light-harvesting materials with dynamical management of light transmittance hold great promise in smart photovoltaics (PV). Here, a novel organic–inorganic halide,  $MVBi_2I_8$  ( $MV$  = methyl viologen cation), exhibiting reversible thermochromism and constant bandgap of  $\approx 1.65$  eV over a wide temperature range of 77–453 K, is presented as a candidate. The compound consists of 0D  $(Bi_4I_{16})^{4-}$  clusters and  $MV^{2+}$  cations. And the adjacent  $(Bi_4I_{16})^{4-}$  clusters are in touch with each other, forming a 3D interaction for the inorganic part. The experimental and theoretical studies reveal that the ionic and covalent interactions in the crystal undergo a self-adjusting process in response to temperature changes. The self-adjustment and electron transfer between inorganic clusters and organic cations enable excellent reversible thermochromism and constant narrow bandgaps over a wide temperature range, which is expected for smart PV windows integrated with information displays and potentially other technologies.

responsiveness to external stimuli, that can be combined with many emerging areas, including architectural windows and information displays, etc.<sup>[1]</sup> Among the external stimuli such as optical, electrical, and temperature, etc., the temperature is the most practical one, not only because of its environmental maneuverability but also because the changes in lattice vibrations it induces are prone to renormalization of electronic structure and discrepancy of photoelectric properties.<sup>[2]</sup> However, the structural and performance stability of most semiconductor materials is difficult to maintain over a sufficiently large temperature range.<sup>[3]</sup> Since smart PV windows should promise the ability of stable solar energy harvesting and efficient electron transfer, it is extremely urgent to break through the material constraints.<sup>[4]</sup>

## 1. Introduction

Smart photovoltaic (PV) windows represent promising properties including switchable transparencies and stable optoelectronic

In the past decade,  $ABX_3$  halide perovskites, represented by  $CsPbX_3$  and  $(CH_3NH_3)PbX_3$  ( $X$  = halide ions), have attracted great interest as a promising class of photovoltaic materials and have rapidly developed into a research hotspot.<sup>[5]</sup> Yang et al. studied the thermochromic properties of  $CsPbI_{3-x}Br_x$  ( $0 \leq x \leq 3$ ) perovskites induced by temperature-affected phase transitions and demonstrated their potential for the smart PV Window.<sup>[6]</sup> Recently, Pb-free halide perovskites become candidates for temperature-controlled smart materials mining due to their excellent stability and low toxicity.<sup>[7]</sup> For example,  $Cs_2AgBiBr_6$  was demonstrated to be a stable reversible thermochromic material because of its convertibility in response to temperature caused by bond length changes.<sup>[8]</sup> However, Pb-free halides tend to have wider bandgaps, especially at lower temperatures, which are detrimental for light harvesting.<sup>[9]</sup> Even the observed color changes are caused by bandgap regulation in many cases.<sup>[10]</sup> Therefore, the transparency of the materials related to light absorption intensity is an issue that deserves to be focused on in the synthesis of candidates for smart PV windows.

Low-dimensional organic–inorganic hybrid halides synthesized by modulation of the A-site of  $ABX_3$  halide perovskites have the potential to be enriched with functionalized optoelectronic diversity.<sup>[11]</sup> In particular, rigid amine, such as 1,1'-disubstituted-4,4'-bipyridinium salts, has been shown to direct the synthesis of quasi-3D lead-free perovskites for desirable bandgaps.<sup>[12]</sup> In organic–inorganic hybrid halides containing both ionic and covalent bonds, the transfer of electrons from the inorganic part to the organic moieties may be strongly influenced by the external temperature, which is expected to endow the compounds with thermochromic properties.


R. Wen, Y. Wang, X. Ma, Y. Yan, Q. Ma, H. Sun, Z. Gao  
Key Laboratory of Applied Surface and Colloid Chemistry MOE  
Xi'an Key Laboratory of Organometallic Material Chemistry  
School of Chemistry and Chemical Engineering  
Shaanxi Normal University  
Xi'an 710119, P. R. China  
E-mail: yyw@snnu.edu.cn; zwgao@snnu.edu.cn

J. Gao  
Department of Chemistry  
University of Michigan  
Ann Arbor, MI 48109, USA

H. Huang  
Department of Microsystems  
University of South-Eastern Norway  
Borre 3184, Norway  
E-mail: huanghao881015@163.com

Z. Gao  
School of Chemistry & Chemical Engineering  
Xinjiang Normal University  
Urumqi 830054, P. R. China

Z. Gao  
Research Institute of Comprehensive Energy Industry Technology  
College of Chemistry & Chemical Engineering  
Yan'an University  
Yan'an, Shaanxi 716000, P. R. China

 The ORCID identification number(s) for the author(s) of this article can be found under <https://doi.org/10.1002/adom.202203148>.

DOI: 10.1002/adom.202203148

Following this conception, we construct a novel bismuth iodide,  $\text{MVBi}_2\text{I}_8(\text{I})$  (the molecular formula is  $\text{C}_{24}\text{H}_{28}\text{N}_4\text{Bi}_4\text{I}_{16}$ , MV = methyl viologen cations), in this work using methyl viologen as a structural direction agent. The structure of its inorganic part presents as isolated OD  $(\text{Bi}_4\text{I}_{16})^{4-}$  clusters, which interact with each other through  $\text{I}\cdots\text{I}$  contact and ensure a narrow bandgap.  $\text{MV}^{2+}$  cations are distributed in the voids of the  $(\text{Bi}_4\text{I}_{16})^{4-}$  clusters to balance the charges.

## 2. Results and Discussion

Compound **1** was synthesized using a solvothermal method by introducing 4,4'-bipyridine in methanol. Scanning electron microscopy (SEM) image showed the polyhedral morphology of compound **1** (Figure S1, Supporting Information). Single crystal X-ray diffraction analyses reveal that it crystallized in a triclinic system with space group  $P\bar{1}$  at 293 K. The crystallographic data are displayed in Tables S1 and S2 (Supporting Information). As shown in Figure 1a, the structure of **1** is composed of  $(\text{Bi}_4\text{I}_{16})^{4-}$  tetranuclear clusters and  $\text{MV}^{2+}$ . The  $(\text{Bi}_4\text{I}_{16})^{4-}$  clusters are formed by linking four  $(\text{BiI}_6)$  octahedra via  $\mu^2$ - or  $\mu^3$ -I ions (Figure 1b). In addition to the  $\mu^2$ - or  $\mu^3$ -I ions, there are ten terminal I ions in the cluster. The  $\text{MV}^{2+}$  cations sit around the inorganic clusters to balance the negative charge of inorganic clusters.

It is the first example of bismuth halides consisting of a tetranuclear  $(\text{Bi}_4\text{I}_{16})^{4-}$  cluster. The Bi–I bond lengths and I–Bi–I angles in  $(\text{Bi}_4\text{I}_{16})^{4-}$  clusters are in the range of 2.88–3.35 Å and

84–97°, respectively, which are common in other bismuth iodide compounds.<sup>[13]</sup> Most notably, the  $(\text{Bi}_4\text{I}_{16})^{4-}$  clusters interact with others through  $\text{I}\cdots\text{I}$  contacts, as the nuclear spacing of some terminal I ions of the neighboring  $(\text{Bi}_4\text{I}_{16})^{4-}$  clusters are between 3.82 and 4.20 Å, significantly shorter than twice the I–radius, that is, 4.40 Å. The contacts of inorganic clusters form a parallelogram frame of interaction along the (001), (010), and (100) directions (Figure 1c,d). This weak 3-D interaction of inorganic clusters is of significance for efficient charge transport based on dimensionality effects for crystals. Rigid  $\text{MV}^{2+}$  cations are inserted into the parallelogram frame in pairs along (010) direction, and each pair is surrounded by four  $(\text{Bi}_4\text{I}_{16})^{4-}$  clusters. The weak interactions between the adjacent  $(\text{Bi}_4\text{I}_{16})^{4-}$  clusters and the ionic forces between  $\text{MV}^{2+}$  and  $(\text{Bi}_4\text{I}_{16})^{4-}$  give the rigid inorganic clusters and  $\text{MV}^{2+}$  cations some flexibility, which is anticipated to contribute to the stability of the crystals.

As expected, thermogravimetric analyses show **1** has almost no weight loss below 557 K, suggesting the good stability of the sample (Figure S2, Supporting Information). Interestingly, the powder X-ray diffraction pattern of **1** is consistent with the simulated one whether exposed to air at ambient conditions for up to one year or after 6 h of heating at 453 K or cooling at 77 K (Figure S3, Supporting Information). These results demonstrate the toughness of **1**, that is, excellent thermal stability and good antioxidative stability, which may be attributed to the flexibility factors of the crystal structure.

Visually, the color of the samples changed from red to dark red and then to almost black-reddish-brown as the temperature increased from 77 to 453 K, showing a distinct thermochromic

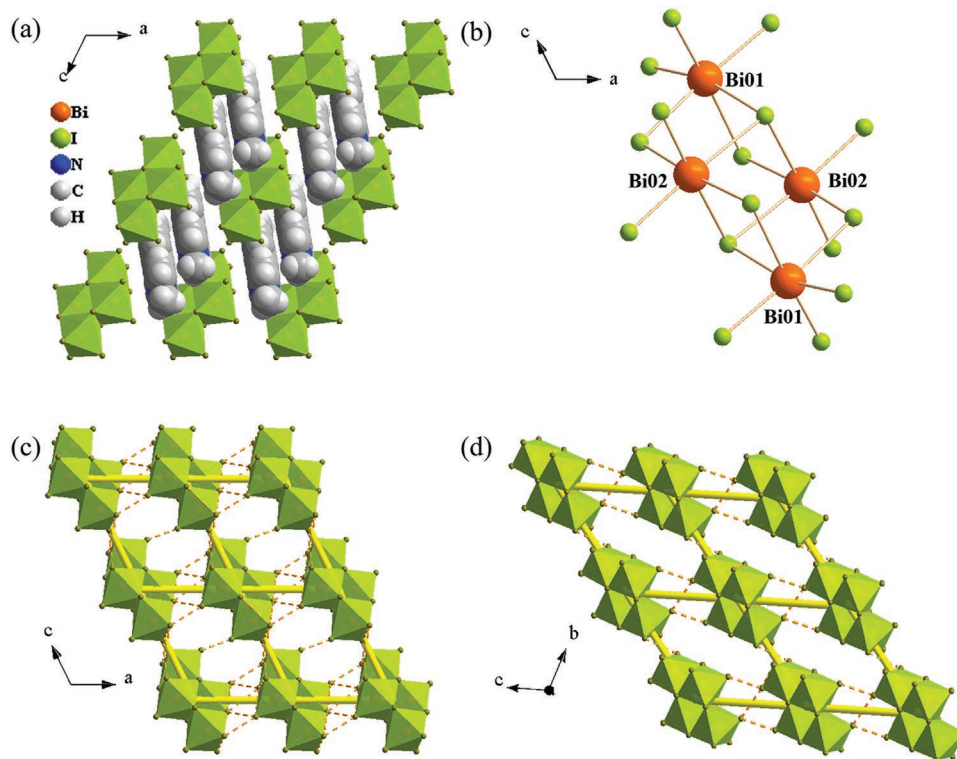


**Figure 1.** Crystal structure of a) **1** viewing along the (010) direction and b) the structure of  $(\text{Bi}_4\text{I}_{16})^{4-}$  cluster; the contacts of inorganic clusters viewing along the c) (010) and d) (100) directions.

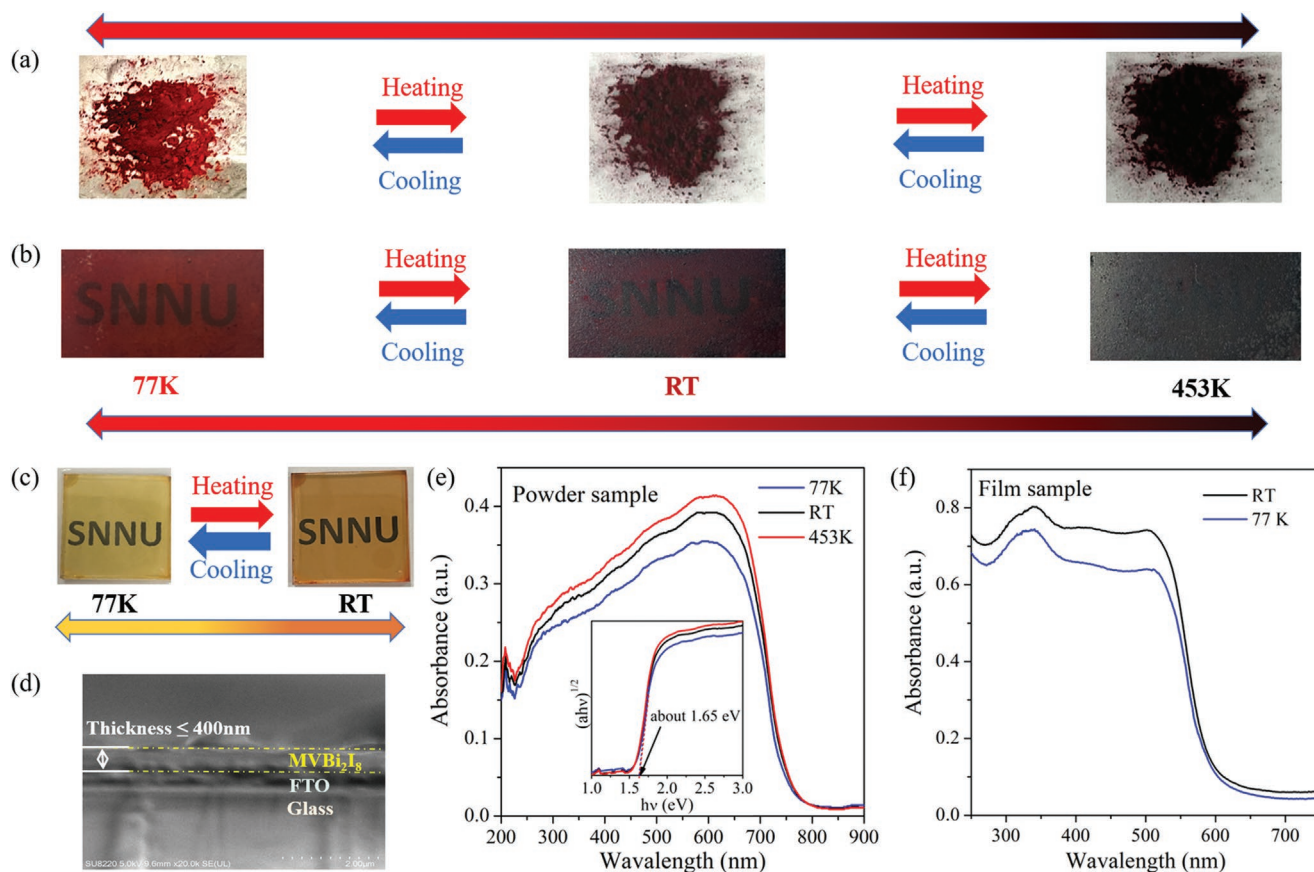


**Figure 2.** Optical images of a) powder and b) drop-coated film at different temperatures; c) optical images of spin-coated film at different temperatures; d) SEM image of cross section of the spin-coated film; e) in situ UV–vis–NIR absorption spectra and corresponding optical bandgaps of the powder sample; f) UV–vis absorption spectra of the film sample on FTO glass.

behavior (Figure 2a). To inspect the potential of this compound as a candidate for smart PV, we fabricated a simple device by dropping an organic solution (DMF: DMSO = 4:1.3) of dissolved **1** onto an FTO glass. Then a deep red film was obtained after annealing (Figure 2b). The XRD pattern of this film is in good agreement with the simulation one, except that the peak at 9.05 is very strong, implying a certain directional growth tendency of the crystals (Figure S4, Supporting Information). Similar to the powder sample, the film exhibits a significant temperature-dependent color change. When we placed a piece of paper labeled “SNNU” under the film, the letters were visible at room temperature (RT) but became clearer at 150K (Figure 2b). As the temperature increased, the word gradually blurred until unrecognizable, demonstrating the thermochromism of the sample. Interestingly, this thermochromic behavior is reversible and persists well after multiple heating-cooling cycles.

As is well known, the color and transparency of a film depend on its thickness and flatness. To increase the transparency of the film, we prepared a high-quality thin film of **1** by spin coating. Obviously, there is a huge chromatic aberration between the spin-coated film and the drop-coated one (Figure 2c). XRD indicated the purity of the crystals on the film (Figure S4, Supporting Information). SEM confirmed that the thickness of the film was  $\approx 400$  nm (Figure 2d). From 77 K

to RT, the color of the film changed from pale yellow to dark yellow, and then becomes pale yellow again after cooling to 77 K. Compared to the powder sample or drop-coated film, the spin-coated film exhibits lighter color and better photopermeability. This result suggests that the specific properties of the film are the potential to be tuned by adjusting the fabrication process of the device without disturbing its properties.

A series of UV–vis–NIR absorption analyses were performed in situ to study the light-harvesting properties of **1** at different temperatures. At RT, the powder sample exhibits an absorption edge end of 800 nm (Figure 2e), indicating that **1** is an outstanding light-harvesting material. Correspondingly, the optical bandgap of **1** at RT estimated by using the  $\text{tauc}$ -plot calculation is  $\approx 1.65$  eV, which is general agreement with the one estimated by reflectance being transformed from absorbance using the Kubelka–Munk function. Interestingly, the absorption edge on the spectrum hardly changed whether the sample was heated up to 453 K or cooled to 77 K. The bandgap was not widened and even tended to narrow somewhat at low temperatures. It is obvious that the intensity of the UV–vis absorption spectrum gradually rises with the increase of the external temperature. Meanwhile, UV–vis absorption analysis was performed on the spin-coated film sample. Due to the difference between the thin film and the powder, the observed absorption edge of the film sample is  $\approx 690$  nm, which is different from the powder sample

(Figure 2f). However, the absorption of the film sample gave a similar trend to that of the powder sample in the response to the temperature change. These results are inconsistent with its thermochromic behavior, which is different from our common belief that darker material should have narrower bandgaps. And the thermochromic property of this sample may be caused by the variation of the absorption intensity of UV–vis light.

In order to disclose the mechanism of the thermochromism, we analyzed the structure of **1** at 150 K by single crystal XRD. It reveals that the structure at low temperatures is very similar to that at RT. Meanwhile, the density functional theory was used to calculate the electronic band structures of **1** at different temperatures (Figure S5, Supporting Information). Theoretical bandgaps demonstrated the peculiar phenomenon of bandgaps slightly narrowing with the decreasing of temperature. The theoretical bandgap of the crystal at RT is  $\approx 1.645$  eV, which is corresponding well with the experimental value of 1.65 eV. While a narrower theoretical bandgap of 1.637 eV was obtained for the crystal at 150 K, which is consistent with the experimental results as well.

By studying the structure of **1** in response to temperature changes, a self-adjustment behavior has been observed for the ionic and covalent interactions in the crystal. Consistent with the law of thermal expansion and cold contraction, the distances between the inorganic clusters and  $MV^{2+}$  cations at low temperatures are shortened, as manifested by a slight decrease in the unit cell volume,  $V = 1398.8(3) \text{ \AA}^3$  versus  $V = 1413.87(8) \text{ \AA}^3$ . The  $I \cdots I$  contacts of cluster-cluster are slightly tighter at low temperatures as well. Two new  $I \cdots I$  contacts are formed along the (011) direction with a distance of 4.32  $\text{ \AA}$  (Figure S6, Supporting Information). However, most Bi–I bond lengths in the  $(Bi_4I_{16})^{4-}$  clusters are even longer at 150 K than at RT (Figure 3a). This is seemingly contrary to our concept of the expansion and contraction of objects with heat. In order to describe atomic-scale vibration for temperature-dependent of compound **1** with structural properties, Ab Initio Molecular Dynamics simulations were carried out at 150 K and RT, respectively. The distribution of  $R_{Bi-I}$  bond lengths was collected by using Gaussian functions fitting (Figure 3b). A subtle fluctuation is observed on the Bi–I lengths that deviate from

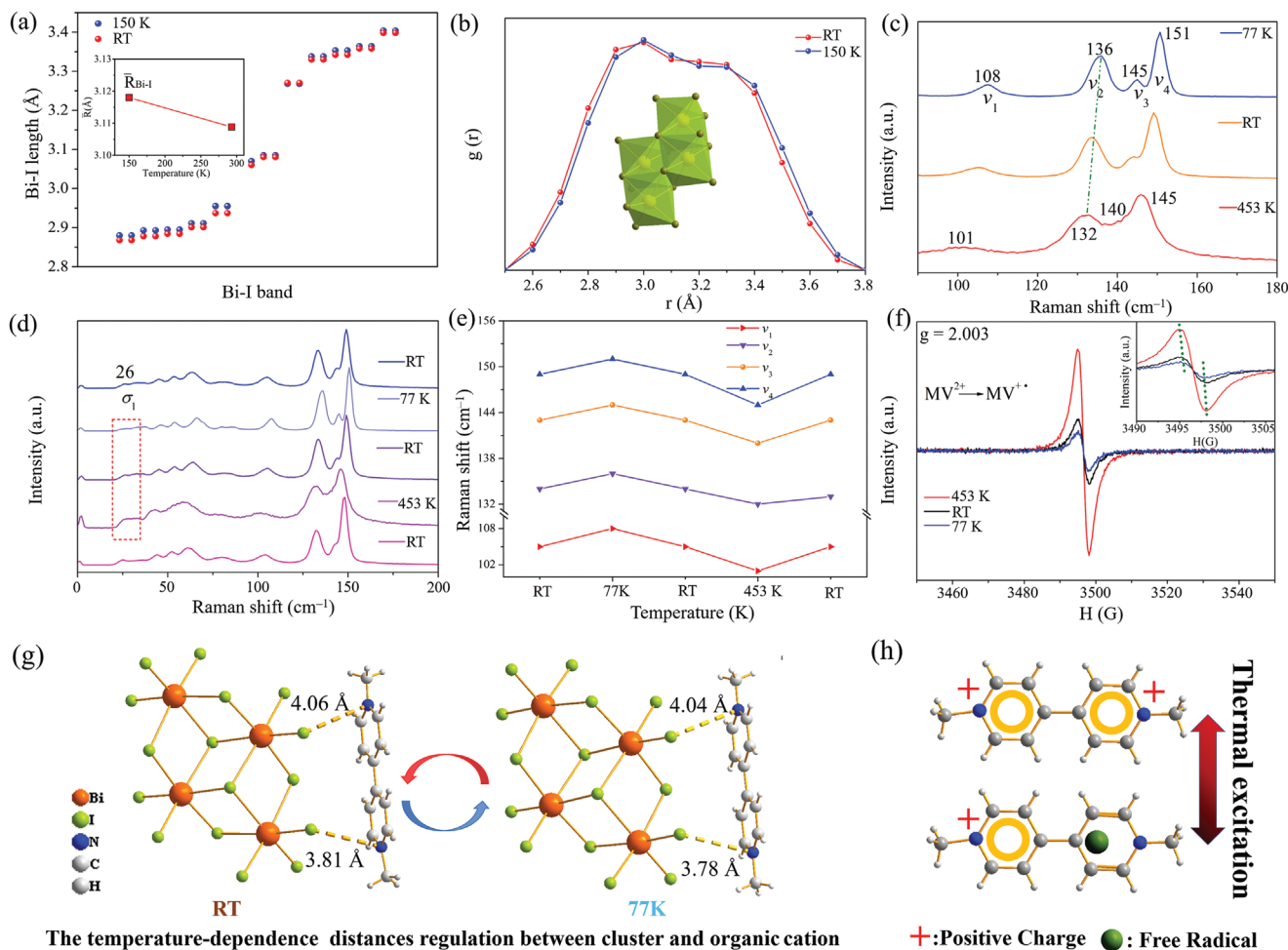


**Figure 3.** a) Bi–I bond lengths and average  $R_{Bi-I}$  of **1** at different temperatures obtained from the crystal data; b) the pair distribution function  $g(r)$  (fitted by Gaussian function) of Bi–I atomic pairs at 150 K and RT; c) in situ Raman spectra of **1** from 77 to 453 K revealing the  $\nu_{Bi-I}$  stretching vibrations; d) in situ Raman spectra of **1** during heating/cooling cycles (RT–77 K–RT–453 K–RT); e) the shift of the signals for  $\nu_{Bi-I}$  on the Raman spectra in (d) at different temperature during heating/cooling cycles; f) in situ ESR spectra of **1** at different temperatures; g) the distances between the inorganic cluster and  $MV^{2+}$  cation at different temperatures; h) thermal excitation behavior of  $MV^{\bullet+}$  radical obtained from  $MV^{2+}$ .

the symmetric Gaussian shape that may be attributed to the diversity of I in the  $(\text{Bi}_4\text{I}_{16})^{4-}$  cluster. Correspondingly, there is a certain rightward shift for the 150 K curve compared with that for RT, which is consistent with the fact that the Bi–I bond tends to lengthen with decreasing temperature.

The variation of Bi–I bond length may be the result of self-adjustment of structure. The  $(\text{Bi}_4\text{I}_{16})^{4-}$  cluster consists of the soft acid  $\text{Bi}^{3+}$  cation containing an 18+2 electron configuration and the soft base  $\text{I}^-$  ion. Based on the soft and hard acid-base theory, a stable covalent force is formed between the  $\text{Bi}^{3+}$  cation and the  $\text{I}^-$  ion, which drives the inorganic cluster to be very stable. The  $\text{MV}^{2+}$  cations are stable as well due to their conjugation property. And the inorganic cluster and organic amine cations interact through ionic bonding, just like two fat people hugging each other. Upon the temperature cooling, the electron become inactive. So the distance between the clusters and amines becomes closer to maintain sufficient Coulomb forces. But the repulsive force between the  $\text{MV}^{2+}$  and  $\text{Bi}^{3+}$  limits the shortening of that distance. In that case, the iodide ion located between them may move slightly away from the Bi to balance this contradiction. The hypothesis is corroborated by the fact that the length of the Bi–I bond in the inorganic cluster becomes longer at 150 K. This self-adjustment phenomenon may be responsible for the enhanced band gap stability.

The temperature-responsive fluctuations of bond lengths were studied by using in situ Raman spectroscopy of the powder samples at different temperatures. As shown in Figure 3c, there are four Raman shifts in the range of 90–180  $\text{cm}^{-1}$ , which may be attributed to the  $\nu_{\text{Bi}-\text{I}}$  stretching vibrations.<sup>[14]</sup> From 77 K to RT and then to 453 K, there is a significant red shift of  $\approx 10 \text{ cm}^{-1}$ , which can be restored after cooling (Figure 3d). The blue shift of  $\nu_{\text{Bi}-\text{I}}$  from RT to 77 K on the Raman shift spectra indicates that the bond energy of Bi–I is enhanced despite its extension during the cooling process. The phenomenon of the extension and enhancement of Bi–I verifies our hypothesis about the self-adjustment of Bi–I in response to the law of cold shrinkage. Correspondingly, the signal  $\approx 26 \text{ cm}^{-1}$  assigned as the bending vibrations of  $\delta_{(\text{I}-\text{Bi}-\text{I})}$  is more pronounced at high temperatures. This may be due to the fact that the crystal tends to be nervous under freezing and become livelier with increasing temperature. The repeatable shifts on the Raman spectra correspond to their reversible thermochromic phenomenon (Figure 3e).

The thermochromism of **1** is mainly promoted by the temperature-dependent electron transfer between the inorganic anion clusters and the organic cations. As shown in Figure 3f, sharp signals are gradually displayed on the electron paramagnetic resonance spectra from 77 to 453 K, and the  $g$  values of 2.003 imply the generation of  $\text{MV}^{2+}$  radicals from  $\text{MV}^{2+}$ .<sup>[15]</sup> This result indicates that the generation of  $\text{MV}^{2+}$  radicals is a thermal excitation process.

Density functional theory was used to calculate the organic and inorganic parts density of states. Comparatively, the valence band is mainly contributed from the inorganic parts, especially iodine, while the conduction band is mostly contributed from the organic part (Figure S7, Supporting Information). Under thermal excitation, electrons may be readily transferred from the  $(\text{Bi}_4\text{I}_{16})^{4-}$  cluster to  $\text{MV}^{2+}$ , leading to the formation of the radical cations.<sup>[16]</sup> As shown in Figure 3g, the closest distances between terminal I of the inorganic cluster and the N of the

$\text{MV}^{2+}$  cation are in the range of 3.78–4.06 Å, which is short enough to allow electron transport. Thus, terminal I near the  $\text{MV}^{2+}$  cation acts as the electron donor, the  $\text{MV}^{2+}$  cation acts as the electron acceptor, and electron-transfer behavior is implemented between the I atom and  $\text{MV}^{2+}$  cation under thermal induction (Figure 3h). The electrons in the conjugated rings of  $\text{MV}^{2+}$  are then rearranged to form  $\text{MV}^{+\cdot}$ , which makes the compound more stable to withstand large temperature changes. The electron transfer between  $(\text{Bi}_4\text{I}_{16})^{4-}$  and  $\text{MV}^{2+}$  is like a cache of energy.

More importantly,  $\text{MV}^{+\cdot}$  cation radicals are a characteristic chromogenic group because of their strong absorption in the visible light region during the intramolecular photoelectron transfer.<sup>[17,18]</sup> The formation of  $\text{MV}^{+\cdot}$  radicals may be responsible for the enhancement of the optical absorption intensity of **1** on the UV–vis–NIR spectra with increasing temperature, although its absorption edge is approximately constant. The idea of using viologens and then creating radical cations for color change has already been demonstrated by N. Mercier et al. more than a decade ago.<sup>[19]</sup> These original papers have important discussions on the mechanisms of photochromism. To test whether **1** has photochromic properties, we irradiated the film samples of **1** with a UV lamp for 24 h. However, there was little change in either the color or the UV–vis absorption spectrum of the film (Figure S8, Supporting Information). In particular, the absorption spectra were almost unchanged in the visible range of 400–600 nm, which further indicates that **1** has no significant photochromic behavior under UV irradiation. This result may be due to the unique 0-D cluster structure of the compound.

To study the temperature-dependent semiconducting properties of **1**, we investigated the conductivities of the compressed tablet of **1** at different temperatures. From RT to 373 K, the conductivity gradually increases from  $1.76 \times 10^{-10}$  to  $1.94 \times 10^{-9} \text{ S cm}^{-1}$ , which is in the range of typical semiconductors (Figure S9, Supporting Information).<sup>[20]</sup> The temperature-dependent conductivity implies that thermal excitation facilitates the transport of charge in this compound. In addition, the photo-conductivity of the tablet sample and the film sample was measured separately with a bias voltage of 10 V under the irradiation of a 300 W xenon lamp. As shown in Figure S10 (Supporting Information), repetitive photo-current responses were observed over several lamps on/off cycles, indicating that **1** is a potential candidate for a light-harvesting material. In contrast, the photoelectric response of the film is more sensitive than that of the tablet, which may be ascribed to the different densities and connectivity of the devices prepared by different methods.

Smart PV window is embodied in dynamical management light transmittance and is becoming increasingly important due to excellent energy-saving capabilities for building energy. However, for the exploitation of halide as smart PV materials, it is still in the development stage. Since the bandgap of halides is determined by the metal halide and the cation, the construction of compounds is crucial in the bandgap engineering related to electron transport, which affects their light-harvesting capabilities. Based on the self-adjusting properties of the crystals observed in this work, it is anticipated to obtain the desired compounds with stable properties by designing

## Organic-Inorganic Halides Chromic Behaviors

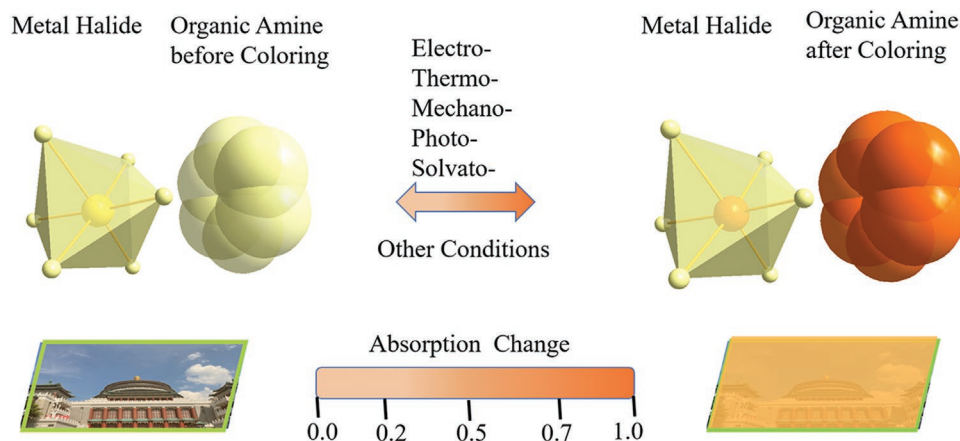


**Figure 4.** A blueprint of coloring strategy for organic–inorganic halides as a smart photovoltaic window.

low-dimensional halides. In addition, besides balancing the charge and stabilizing the structure, cations with conjugation are expected to take on additional tasks, such as coloring. Therefore, it is potential to acquire halides with electro-, thermo-, mechano-, photochromics, and other chromics features by choosing some organic amines, such as aniline, diimidazolium, *N,N*'-dimethyl-1,4-diazoniabicyclo(2.2.2)octonium, protonation pyridine, etc. (Figure 4).<sup>[16,17,21]</sup>

### 3. Conclusion

In summary, we present a novel organic–inorganic halide,  $MVBi_2I_8$ , as a light-harvesting candidate for smart PV windows. This halide features excellent thermal stability, constant bandgap, and reversible thermochromic behavior in the temperature range from 77 to 453 K, which meet key requirements for smart PV windows. The compound consists of 0-D ( $Bi_4I_{16}$ )<sup>4-</sup> clusters with 3-D interactions and  $MV^{2+}$  cations that fill the space in pairs. The structure-activity relationship of the crystal was studied by single crystal analyses, in situ Raman spectroscopy, and density functional theory calculation. It was found that the crystal structure was self-adjusted against temperature changes. The excellent thermal stability and constant bandgap of  $MVBi_2I_8$  may be attributed to the self-adjustment of the crystal. The thermochromism is ascribed to the formation of  $MV^{+}$  cation radicals caused by the transfer of electrons from the inorganic clusters to the organic cations in the process of self-adjusting. The self-adjustment characteristics of crystals revealed in this work are the potential to guide the synthesis of halide for switchable optoelectronics.

### Supporting Information

Supporting Information is available from the Wiley Online Library or from the author.

### Acknowledgements

This work was financially supported by the National Natural Science Foundation of China (21771122, 22271179, 22002083), the Key Research and Development Projects of Shaanxi Province (2023-YBGY-471), the 111 Project (B14041), the Key Research and Development Program in Shaanxi Province of China (2021GY-308), the Fundamental Research Funds for the Central Universities (GK202103027) and the MSCA-IF-2020-Individual Fellowships (101024758).

### Conflict of Interest

The authors declare no conflict of interest.

### Data Availability Statement

The data that support the findings of this study are available in the supplementary material of this article.

### Keywords

bandgaps, hybrid halides, self-adjustment, smart photovoltaics, thermochromism

Received: January 30, 2023  
Published online: March 17, 2023

- [1] a) R. Baetens, B. P. Jelle, A. Gustavsen, *Sol. Energy Mater. Sol. Cells* **2010**, *94*, 87; b) A. Llordés, G. Garcia, J. Gazquez, D. J. Milliron, *Nature* **2013**, *500*, 323; c) G. Cai, J. Wang, P. S. Lee, *Acc. Chem. Res.* **2016**, *49*, 1469; d) Y. Ke, C. Zhou, Y. Zhou, S. Wang, S. H. Chan, Y. Long, *Adv. Funct. Mater.* **2018**, *28*, 1800113; e) H. Khandelwal, A. P. H. J. Schenning, M. G. Debije, *Adv. Energy Mater.* **2017**, *7*, 1602209; f) Y. Zhang, C. Y. Tso, J. S. Iñigo, S. Liu, H. Miyazaki, C. Y. H. Chao, K. M. Yu, *Appl. Energy* **2019**, *254*, 113690.
- [2] a) D. Ghosh, D. Acharya, L. Zhou, W. Nie, O. V. Prezhdo, S. Tretiak, A. J. Neukirch, *J. Phys. Chem. Lett.* **2019**, *10*, 5000; b) H. Fu, C. Jiang,

- C. Luo, H. Lin, H. Peng, *Eur. J. Inorg. Chem.* **2021**, 2021, 4984; c) B. Sun, X. F. Liu, X. Y. Li, Y. Cao, Z. Yan, L. Fu, N. Tang, Q. Wang, X. Shao, D. Yang, H. L. Zhang, *Angew. Chem., Int. Ed.* **2020**, 59, 203; d) Y. Ke, J. Chen, G. Lin, S. Wang, Y. Zhou, J. Yin, P. S. Lee, Y. Long, *Adv. Energy Mater.* **2019**, 9, 1902066; e) W. Zhang, Z. Sun, J. Zhang, S. Han, C. Ji, L. Li, M. Hong, J. Luo, *J. Mater. Chem. C* **2017**, 5, 9967.
- [3] a) B. Conings, J. Drijkoningen, N. Gauquelin, A. Babayigit, J. D'Haen, L. D'Olieslaeger, A. Ethirajan, J. Verbeeck, J. Manca, E. Mosconi, F. D. Angelis, H.-G. Boyen, *Adv. Energy Mater.* **2015**, 5, 1500477; b) K. Hong, Q. V. Le, S. Y. Kim, H. W. Jang, *J. Mater. Chem. C* **2018**, 6, 2189.
- [4] a) Z. Ma, Z. Liu, S. Lu, L. Wang, X. Feng, D. Yang, K. Wang, G. Xiao, L. Zhang, S. A. T. Redfern, B. Zou, *Nat. Commun.* **2018**, 9, 4506; b) X. Jing, D. Zhou, R. Sun, Y. Zhang, Y. Li, X. Li, Q. Li, H. Song, B. Liu, *Adv. Funct. Mater.* **2021**, 31, 2100930; c) J. Di, L. Li, Q. Wang, J. Yu, *CCS Chem.* **2021**, 3, 2280; d) C. Sun, Z. Liu, S. Wang, H. Pang, R. Bai, Q. Wang, W. Chen, A. Zheng, W. Yan, J. Yu, *CCS Chem.* **2021**, 3, 189.
- [5] a) M. Grätzel, *Nat. Mater.* **2014**, 13, 838; b) X. Li, D. Q. Bi, C. Y. Yi, J. D. Décoppet, J. S. Luo, S. M. Zakeeruddin, A. Hagfeldt, M. Grätzel, *Science* **2016**, 353, 58.
- [6] J. Lin, M. Lai, L. Dou, C. S. Kley, H. Chen, F. Peng, J. Sun, D. Lu, S. A. Hawks, C. Xie, F. Cui, A. P. Alivisatos, D. T. Limmer, P. Yang, *Nat. Mater.* **2018**, 17, 261.
- [7] A. Babayigit, A. Ethirajan, M. Muller, B. Conings, *Nat. Mater.* **2016**, 15, 247.
- [8] W. Ning, X. G. Zhao, J. Klarbring, S. Bai, F. Ji, F. Wang, S. I. Simak, Y. Tao, X. M. Ren, L. Zhang, W. Huang, I. A. Abrikosov, F. Gao, *Adv. Funct. Mater.* **2019**, 29, 1807375.
- [9] V. R. Shayapov, A. N. Usoltsev, S. A. Adonin, M. N. Sokolov, D. G. Samsonenko, V. P. Fedin, *New J. Chem.* **2019**, 43, 3927.
- [10] a) W. Zhang, X. Ji, B. J. Peng, S. Che, F. Ge, W. Liu, M. Al-Hashimi, C. Wang, L. Fang, *Adv. Funct. Mater.* **2019**, 30, 1906463; b) Y. Fang, L. Zhang, L. Wu, J. Yan, Y. Lin, K. Wang, W. L. Mao, B. Zou, *Angew. Chem., Int. Ed.* **2019**, 58, 15249.
- [11] a) Y. Shi, Z. Ma, D. Zhao, Y. Chen, Y. Cao, K. Wang, G. Xiao, B. Zou, *J. Am. Chem. Soc.* **2019**, 141, 6504; b) C. Ji, S. Wang, L. Li, Z. Sun, M. Hong, J. Luo, *Adv. Funct. Mater.* **2019**, 29, 1805038; c) K. Tao, Y. Li, C. Ji, X. Liu, Z. Wu, S. Han, Z. Sun, J. Luo, *Chem. Mater.* **2019**, 31, 5927; d) R. Wen, X. Ma, K. Zhang, X. Zhang, Q. Gu, H. Sun, Y. Jian, G. Zhang, Y. Wang, Z. Gao, *Inorg. Chem.* **2022**, 61, 8521; e) N. Mercier, N. Louvain, W. Bi, *CrystEngComm* **2009**, 11, 720.
- [12] Y. Wang, R. Wen, Y. Liu, L. Y. Bi, M. Yang, H. Sun, Y. Z. Zheng, G. Zhang, Z. Gao, *ChemSusChem* **2020**, 13, 2753.
- [13] a) L. Yao, G. Niu, L. Yin, X. Du, Y. Lin, X. Den, J. Zhang, J. Tang, *J. Mater. Chem. C* **2020**, 8, 1239; b) M.-Q. Li, Y.-Q. Hu, L.-Y. Bi, H.-L. Zhang, Y. Wang, Y.-Z. Zheng, *Chem. Mater.* **2017**, 29, 5463; c) L.-Y. Bi, Y.-Q. Hu, M.-Q. Li, T.-L. Hu, H.-L. Zhang, X.-T. Yin, W.-X. Que, M. S. Lassoued, Y.-Z. Zheng, *J. Mater. Chem. A* **2019**, 7, 19662.
- [14] a) M. Wojtaś, R. Jakubas, J. Baran, *Vib. Spectrosc.* **2005**, 39, 23; b) S. Öz, J.-C. Hebig, E. Jung, T. Singh, A. Lepcha, S. Olthof, F. Jan, Y. Gao, R. German, P. H. M. van Loosdrecht, K. Meerholz, T. Kirchartz, S. Mathur, *Sol. Energy Mater. Sol. Cells* **2016**, 158, 195; c) S. M. Jain, D. Phuyal, M. L. Davies, M. Li, B. Philippe, C. De Castro, Z. Qiu, J. Kim, T. Watson, W. C. Tsoi, O. Karis, H. Rensmo, G. Boschloo, T. Edvinsson, J. R. Durrant, *Nano Energy* **2018**, 49, 614.
- [15] H. Yoshikawa, S.-i. Nishikiori, T. Watanabe, T. Ishida, G. Watanabe, M. Murakami, K. Suwinska, R. Luboradzki, J. Lipkowski, *J. Chem. Soc., Dalton Trans.* **2002**, 1907.
- [16] C. Sun, M. S. Wang, P. X. Li, G. C. Guo, *Angew. Chem., Int. Ed.* **2017**, 56, 554;
- [17] N. Jordão, L. Cabrita, F. Pina, L. C. Branco, *Chem. - Eur. J.* **2014**, 20, 3982.
- [18] a) R. G. Lin, G. Xu, G. Lu, M. S. Wang, P. X. Li, G. C. Guo, *Inorg. Chem.* **2014**, 53, 5538; b) T. M. Bockman, J. K. Kochi, *J. Org. Chem.* **1990**, 55, 4127.
- [19] a) W. Bi, N. Leblanc, N. Mercier, P. Auban-Senzier, C. Pasquier, *Chem. Mater.* **2009**, 21, 4099; b) N. Leblanc, W. Bi, N. Mercier, P. Auban-Senzier, C. Pasquier, *Inorg. Chem.* **2010**, 49, 5824; c) Q. Pan, M. Sun, C. Zhang, L. Li, H. Liu, K. Li, H. Li, S. Zang, *Chem. Commun.* **2021**, 57, 11394.
- [20] a) B. Yang, X. Mao, F. Hong, W. Meng, Y. Tang, X. Xia, S. Yang, W. Deng, K. Han, *J. Am. Chem. Soc.* **2018**, 140, 17001; b) S. Wang, L. Li, W. Weng, C. Ji, X. Liu, Z. Sun, W. Lin, M. Hong, J. Luo, *J. Am. Chem. Soc.* **2020**, 142, 55.
- [21] a) A. García-Fernández, I. Marcos-Cives, C. Platas-Iglesias, S. Castro-García, D. Vázquez-García, A. Fernández, M. Sánchez-Andújar, *Inorg. Chem.* **2018**, 57, 7655; b) J. C. Liu, W. Q. Liao, P. F. Li, Y. Y. Tang, X. G. Chen, X. J. Song, H. Y. Zhang, Y. Zhang, Y. M. You, R. G. Xiong, *Angew. Chem., Int. Ed.* **2020**, 59, 3495.